

Data-driven discovery of relevant information in quantum simulators

R. Verdel,^{1,*} V. Vitale,^{1,2,3} R. K. Panda,^{1,2,4} E. D. Donkor,^{1,2} A. Rodriguez,^{1,5}
S. Lannig,⁶ Y. Deller,⁶ H. Strobel,⁶ M. K. Oberthaler,⁶ and M. Dalmonte^{1,2}

¹*The Abdus Salam International Centre for Theoretical Physics (ICTP), Strada Costiera 11, 34151 Trieste, Italy*

²*SISSA—International School of Advanced Studies, Via Bonomea 265, 34136 Trieste, Italy*

³*Université Grenoble Alpes, CNRS, Laboratoire de Physique et
Modélisation des Milieux Condensés (LPMMC), Grenoble 38000, France*

⁴*INFN Sezione di Trieste, Via Valerio 2, 34127 Trieste, Italy*

⁵*Dipartimento di Matematica e Geoscienze, Università degli Studi di Trieste, via Alfonso Valerio 12/1, 34127, Trieste, Italy*

⁶*Kirchhoff-Institut für Physik, Universität Heidelberg,
Im Neuenheimer Feld 227, 69120 Heidelberg, Germany*

(Dated: July 20, 2023)

Quantum simulators offer powerful means to investigate strongly correlated quantum matter. However, interpreting measurement outcomes in such systems poses significant challenges. Here, we present a theoretical framework for information extraction in synthetic quantum matter, illustrated for the case of a quantum quench in a spinor Bose-Einstein condensate experiment. Employing non-parametric unsupervised learning tools that provide different measures of information content, we demonstrate a system-agnostic approach to identify dominant degrees of freedom. This enables us to rank operators according to their relevance, akin to effective field theory. To characterize the corresponding effective description, we then explore the intrinsic dimension of data sets as a measure of the complexity of the dynamics. This reveals a simplification of the data structure, which correlates with the emergence of time-dependent universal behavior in the studied system. Our assumption-free approach can be immediately applied in a variety of experimental platforms.

Introduction.—Recent remarkable advances in highly controlled synthetic quantum devices have revolutionized the study of strongly correlated systems [1–6]. A key element of many of such platforms is their capacity to produce large data sets of many-body snapshots, for example, via generalized projective measurements of the entire wave function [7]. However, the analysis of such outcome poses in general serious challenges, which typically force us to rely on assumptions for certain quantities, disregarding part of the information content of the generated data—in data science language, a dimensional reduction with an uncontrolled loss of information. A particularly important problem is the identification of the most informative observables to describe such quantum many-body systems—a paramount task at the core of quantum field theory [8, 9], that is even more daunting for systems driven out of equilibrium. To address this, one needs to develop methods to process the maximum amount of information in quantum simulator output, which are able to identify relevant features—and thus degrees of freedom—emerging from the underlying physical system, without making any assumption nor uncontrolled dimensional reduction.

In this work, we introduce a theoretical framework for data-driven information discovery in quantum simulation, which is schematically illustrated in Fig. 1. We start by considering collections of independent quantum simulator snapshots, which resolve, for example, the dynamics of a many-body system in space and time [Fig. 1(a)]. Such data sets are characterized using non-parametric unsupervised learning methods [Fig. 1(b)]. Finally, from this system-agnostic and unsupervised description of the

data, we infer relevant information for the physical system under study [Fig. 1(c)].

This framework is based on three techniques: (i) spectral entropies calculated from a principal component analysis (PCA) of the data, (ii) the information imbalance between a subset and the full set of observations, and (iii) the intrinsic dimension of the concomitant data manifolds. These tools which quantify—from different angles—the information content and correlations in the data, have found several successful applications in various fields, such as chemical and biomolecular science [10–18], ecology [19], stock market dynamics [20–25], and image analysis [26–29].

To demonstrate the capabilities of our approach we apply it to experimental data of a spinor Bose-Einstein condensate (BEC) [30]: we evaluate the full set of experimentally measured densities without knowledge of the post-processing steps which are necessary in order to infer the relevant spin variables from them. Our main results are as follows: (I) PCA spectral entropies and information imbalance allow for a theory-agnostic determination of the most informative measured observables. The predictive power of these methods is demonstrated by showing that they can also unveil combinations of the measured densities, which are key to describe the spin structure of the system [30–32]. (II) The behavior of the intrinsic dimension as a function of time, displays a rapid decay to significantly smaller values, after which it features very long, stable plateaus. As argued below, this observation is in strong agreement with the formation of spin structure and the emergence of self-similar dynamics [30, 31, 33–35].

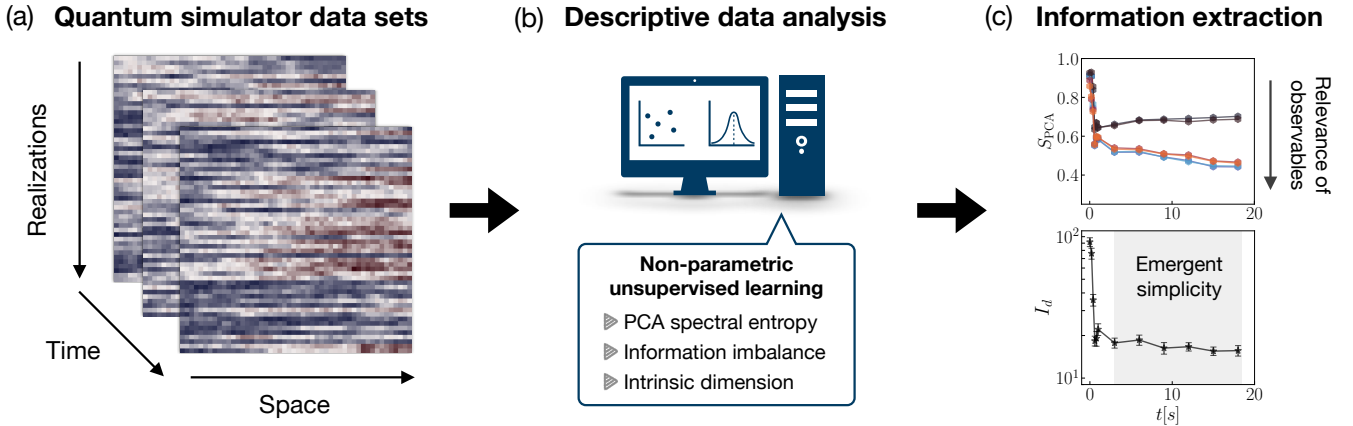


FIG. 1. **Assumption-free unveiling of relevant information in quantum simulation.** (a) We start from snapshots of a many-body system, which are represented as 2D arrays at different times. At a fixed time, each row corresponds to a different realization, while each column is a different data feature, e.g., the atomic density in a given magnetic substate at a given spatial location. (b) Using non-parametric unsupervised learning tools, we perform an exploratory analysis to uncover interesting features of the data, without making any assumptions. (c) From this description, we infer relevant properties of the physical system: (Upper panel) By quantifying the information content of different observables, the spectral entropy of the sample covariance matrix provides a metric to rank the latter according to the strength of the correlations captured by them, thence guiding the identification of relevant (i.e., most informative) degrees of freedom. (Lower panel) After a quick fall to relatively small values, the intrinsic dimension of data sets features a long, stable plateau as a function of time (shaded region), providing a lower bound for the timescale after which the dynamics may become simpler and be captured by universal scaling.

Quantum simulation on a spinor BEC and data sets.— We consider the dynamics realized by a BEC of ^{87}Rb in the $F = 1$ hyperfine spin ground state manifold confined in a quasi-one-dimensional elongated harmonic dipole trap (the data evaluated here are taken from [30]; see this publication for further details on the experiment). The system is initialized with all atoms in the magnetic substate $m_F = 0$. By instantaneously changing a control parameter we tune spin-changing collision processes into resonance. This procedure implements a quench across a quantum phase transition which brings the system far from equilibrium. For different times t after the quench we simultaneously infer the two orthogonal spin projections F_x and F_y from the observed densities with spatial resolution along the longitudinal trap direction [7] via

$$\begin{aligned} F_x &= (n_{1,+1} - n_{1,-1}) / (n_{1,+1} + n_{1,0} + n_{1,-1}), \\ F_y &= (n_{2,+2} - n_{2,-2}) / (n_{2,+2} + n_{2,0} + n_{2,-2}), \end{aligned} \quad (1)$$

where n_{F,m_F} is the density in the state with hyperfine manifold F and magnetic sublevel m_F . At the final parameters of the quench, which places the system into the regime of the easy-plane ferromagnetic phase [32], these define the transverse spin field $F_{\perp} = F_x + iF_y$ [36]. Here, the interplay between energy offsets and spin interactions favor a finite transverse magnetization. During the dynamics the transverse spin field approaches its ground state distribution, which manifests itself in the formation of a ring in the transverse spin histogram after approximately 1–3 s, as shown in Fig. 2(b). Nevertheless, in this regime the system is still highly excited and trans-

verse spin phase excitations evolve dynamically in a self-similar fashion [31]. Such relaxation dynamics is quite rich but complex, making a controlled microscopic characterization extremely challenging. In fact, the interpretation above is motivated by heuristic arguments. The key point we are interested in here is to laid such description based solely on experimental observations, analyzed in a blind-folded manner. That is, we wish to extract essential descriptive elements (most important operators and complexity of the dynamics) without relying on any assumption.

At each evolution time, we obtain a data set with $N_r = 225$ independent realizations for each of the measured densities [see Eq. (1)]. Such data sets are denoted by a matrix $\mathbf{M}^{\alpha}(t) = \{\vec{\mathcal{N}}_1^{\alpha}(t), \vec{\mathcal{N}}_2^{\alpha}(t), \dots, \vec{\mathcal{N}}_{N_r}^{\alpha}(t)\}$, where each row $\vec{\mathcal{N}}_i^{\alpha}(t)$ contains the spatial density profile of a single realization in one of the considered internal states, succinctly labelled here by $\alpha = (F, m_F)$. Each density is linearly sampled at 184 spatial locations, which gives the number of *features* (entries) of each vector $\vec{\mathcal{N}}_i^{\alpha}(t)$. Further, we also consider *joint* data sets formed by concatenating horizontally subsets of the original data sets at a given time. More specifically, each row in a joint data set is formed by appending, one after the other, single realizations of the observables of choice. Thus, for example, if we combine all six densities, the resulting data sets will contain $184 \cdot 6 = 1104$ columns and N_r rows. The particular order in which we concatenate the combined observables is irrelevant for our methods. When needed, we will simply specify joint data sets by using the symbol

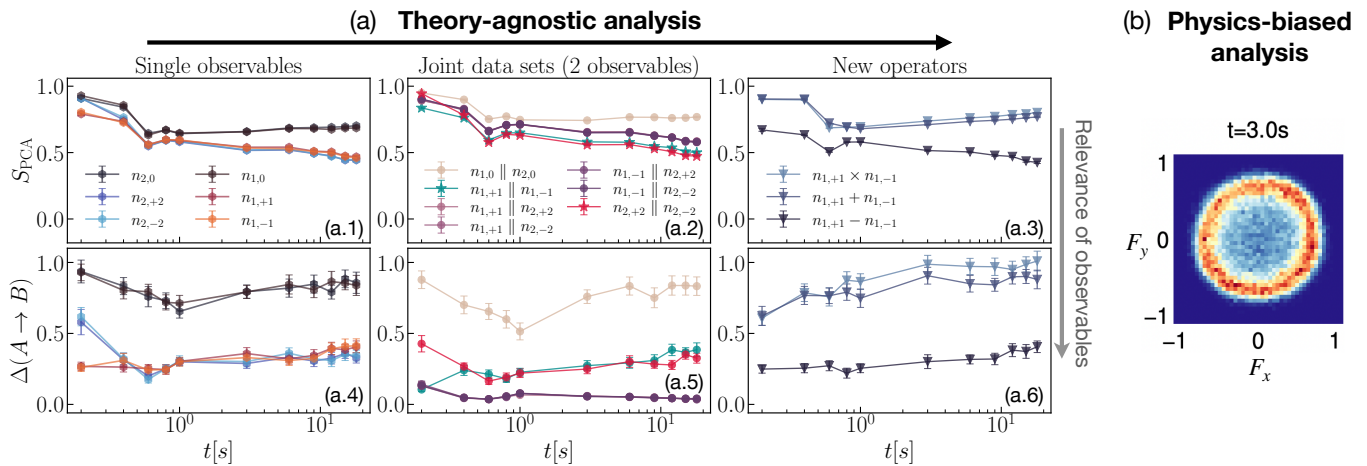


FIG. 2. **Assumption-free identification of relevant observables.** (a) PCA entropy, S_{PCA} , and information imbalance, $\Delta(A \rightarrow B)$, as metrics of relevance: lower values of S_{PCA} signal stronger correlations within a data set, while lower values of $\Delta(A \rightarrow B)$ indicate that more information—from the *full* space of observations—is retained by the features of a given data set. Both metrics clearly show that $n_{1,\pm 1}$ and $n_{2,\pm 2}$ are more relevant (in the sense above) over the full evolution [panels (a.1) and (a.4)]. Identification of relevant groups is also possible by analysing joint data sets: for pairs of observables, $n_{1,+1} \parallel n_{1,-1}$ and $n_{2,+2} \parallel n_{2,-2}$, have a lower S_{PCA} [\star markers in panel (a.2)], and are hence more relevant than any other pair (see ranking of all possible pairs in Ref. [37]). Information imbalance provides a complementary view on the relevance of such pairs, namely, the full space of measured observables is better described if features from both relevant pairs are considered simultaneously [points with $\Delta(A \rightarrow B) \sim 0$ in panel (a.5), corresponding to the joint data sets $n_{1,\pm 1} \parallel n_{2,\pm 2}$. Note that the points of the latter four data sets lie on top of each other—they are equally informative—, both in panel (a.2) and (a.5)]. Finally, we can rank new operators defined from the identified relevant pairs, as illustrated here for a few combinations of $n_{1,+1}$ and $n_{1,-1}$, with their difference $n_{1,+1} - n_{1,-1}$ being more relevant [panels (a.3) and (a.6)]. (b) Histogram of the transverse spin variable in the $F_x - F_y$ plane at $t = 3s$, featuring a ring-like structure. Based on physical arguments [30–32], this variable is the relevant field to describe the quenched system. Our theory-agnostic approach identifies the relevant observables from which this variable is inferred [see Eq. (1)], hence cross-validating the latter analysis.

of the corresponding observables joined by “ \parallel ”.

Assumption-free identification of relevant observables.—We now perform a descriptive analysis of the data sets above, with the task of identifying the most informative observables. We start by introducing a PCA-based spectral entropy. PCA is a non-parametric approach that uses an orthogonal transformation to seek for the directions along which the data exhibit more variation [38, 39]. This problem can equivalently be posed in terms of a singular value decomposition (SVD) of the column-centred data matrix \mathbf{M}^* (where the mean value of each column is subtracted from the entries in the column). (For simplicity, we have omitted the observable and time indices of our previous notation). This allows to find the eigenvalues of the covariance matrix $\Sigma = \mathbf{M}^{*T} \mathbf{M}^* / (N_r - 1)$, that is, $\Sigma \vec{w}_k = \lambda_k \vec{w}_k$, with $\lambda_1 \geq \lambda_2 \geq \dots \geq \lambda_R \geq 0$ (R is the rank of \mathbf{M}^*). The eigenvalues give a measure for the variance of the data along the principal axes, determined by the corresponding eigenvectors. We then define the normalized eigenvalues $\tilde{\lambda}_k := \lambda_k / \sum_k \lambda_k$ [40]. By construction, $\tilde{\lambda}_k \geq 0$ and $\sum_{k=1}^R \tilde{\lambda}_k = 1$. The *PCA spectral entropy* can be thus defined in analogy to

Shannon’s entropy [41], namely,

$$S_{\text{PCA}} := -\frac{1}{\ln(R)} \sum_{k=1}^R \tilde{\lambda}_k \ln(\tilde{\lambda}_k), \quad (2)$$

where for convenience we have normalized by its maximum possible value, $\ln(R)$, which is obtained for a flat eigenvalue distribution. Thus, for a perfectly uncorrelated process (e.g. white noise), $S_{\text{PCA}} = 1$. Instead, for data with correlations among the variables $S_{\text{PCA}} < 1$. This quantity can hence be used as a measure for ranking observables according to their information content (strength of their correlations).

As a second way to quantify the information content of observations, we compute their *information imbalance* in terms of distance ranks (for details see Refs. [13, 14, 37]). As opposed to PCA, this method is not based on a linear transformation; instead, it quantifies the relative information content between different distance measures. Concretely, given a data set with N_r points and \mathcal{F} features, one defines distance measures A and B between data points on two subsets of the feature space and computes the corresponding rank matrices $R_{ij}^{A/B}$, such that $R_{ij}^{A/B} = m$ if j is the m -th nearest neighbor of i (according to A/B). The information imbalance—from A

to B —can then be estimated as the average rank in B restricted to nearest neighbors in A , that is

$$\Delta(A \rightarrow B) \approx \frac{2}{N_r^2} \sum_{i,j:R_{ij}^A=1} R_{ij}^B. \quad (3)$$

With this definition, one can show that when the ranks computed with the two metrics are consistent with each other $\Delta(A \rightarrow B) \sim 0$ (A captures B reliably), whereas when they are fully uncorrelated $\Delta(A \rightarrow B) \sim 1$ (A cannot predict B) [13, 14, 37]. Here, we consider the joint data sets of the six measured observables (data points have $184 \cdot 6 = 1104$ coordinates). Space A is formed by the subset features corresponding to, for example, a single observable or a pair of observables (in which cases, we compute distances using only 184 or $184 \cdot 2 = 368$ coordinates, respectively), while B is chosen as the full space of features. This way, the information imbalance from A to B gives us a direct measure of the relevance of observables and their combinations to describe the full space of observations. Throughout this work, we use the Euclidean metric to compute distances between data points.

Our main results are shown in Fig. 2(a). Let us first analyze the results for the PCA entropy [panels (a.1)–(a.3)]. A clear separation between two groups of observables is noted as the system evolves [panel (a.1)], with $n_{1,\pm 1}$ and $n_{2,\pm 2}$ yielding lower values of S_{PCA} . According to the interpretation above, we conclude that these observables capture stronger correlations and are hence more relevant. Next, we consider joint data sets of two different observables [panel (a.2)]. The most relevant pairs according to this analysis are $n_{1,+1} \| n_{1,-1}$ and $n_{2,+2} \| n_{2,-2}$. The latter result is in excellent agreement with the physics-motivated analysis, in which such observables play a key role in the definition of the transverse spin [see Eq. (1) and Fig. 2(b)]. (The densities $n_{1,0}$ and $n_{2,0}$, are only important for normalization.) Going one step further, in panel (a.3) we explore the relevance of concrete functional combinations of the pair $\{n_{1,+1}, n_{1,-1}\}$ (similar results hold for $\{n_{2,+2}, n_{2,-2}\}$). We find that the difference $n_{1,+1} - n_{1,-1}$ has the lowest S_{PCA} , once again in remarkable agreement with the physics-motivated *ansatz* [42].

We now turn our attention to the information imbalance analysis [panels (a.4)–(a.6)]. These results are completely consistent with the analysis above based on S_{PCA} , and provide a complementary view on the relevance of observables. In fact, in panel (a.4), we can see that the observables with a lower PCA entropy have also a lower information imbalance; thus, they retain more information of the full space of features. Interestingly, in the analysis of pairs of observables [panel (a.5)], we note that in order to capture the full space of observations, one needs to consider features from both relevant pairs. Indeed, we see that the joint data sets $n_{1,\pm 1} \| n_{2,\pm 2}$ have $\Delta(A \rightarrow B) \sim 0$ for the full evolution [note that the points of those data sets are on top of each other in panel (a.5)

of Fig. 2]. The new operator $n_{1,+1} - n_{1,-1}$ has also a significantly lower information imbalance, compared to other combinations [panel (a.6)].

In Ref. [37], we show results for other possible joint data sets. We also include details on the subsampling analysis [43, 44] used for the estimation of error bars.

Complexity evolution of data sets.—We now provide a further characterization of the data sets. Specifically, we study their *intrinsic dimension* I_d , at the considered evolution times. The I_d quantifies the minimum number of variables needed to describe the data [15, 45, 46], thereby providing a measure of their (Kolmogorov) complexity [47–50]. Here we use a distance-based I_d estimator, namely, the TWO-NN algorithm [15], which works as follows. For each point \tilde{N}_i in a generic data set, we compute the distance to its first and second nearest neighbors, denoted by r_{i_1}, r_{i_2} . Next, we define the ratio $\mu_i := r_{i_2}/r_{i_1}$. For data points that are locally uniformly distributed on a I_d -dimensional hypersphere, the distribution of μ is given by $f(\mu) = I_d \mu^{-I_d-1}$ [15]. The cumulative distribution function $F(\mu)$, then satisfies

$$-\ln[1 - F(\mu)] = I_d \ln(\mu), \quad (4)$$

which is used to estimate I_d through a linear fit of the points $\{(\ln(\mu), -\ln[1 - F_{\text{emp}}(\mu)])\}$, where $F_{\text{emp}}(\mu)$ is the empirical cumulate [37].

Shown in Fig. 3(a) is the plot of I_d as a function of time, of the data sets corresponding to the identified relevant operators, $n_{1,+1} - n_{1,-1}$ and $n_{2,+2} - n_{2,-2}$. We observe the same trend in both instances: a quick decay of I_d to considerably smaller values, subsequently displaying long, stable plateaus. The reduction of the I_d signals a simplification of the data structure due to the buildup of correlations among the input variables. The latter is a direct manifestation of the correlations among the elementary constituents of the system. From the physical viewpoint, the post-quench correlations are associated with the formation of a ring-like structure, with approximately constant radius, in the transverse component of the collective spin degree of freedom (insets) [30, 31]. In turn, spatial correlations of the spin phase excitations exhibit universal scaling dynamics [31]. In the present experiment, the universal scaling regime starts approximately at $t \sim 5s$ [30]. The physical basis for such scaling evolution is a dynamical reduction of the relevant parameters in the system. This is strongly consistent with the observed structural simplification of the data, as also observed in recent studies of critical behavior—in and out of equilibrium—in classical and quantum statistical mechanics systems [50–53]. Therefore, in the present case, the observed I_d plateau provides a theory-agnostic lower bound for the timescale after which the dynamics may become simpler, allowing for the emergence of self-similar behavior.

Importantly, this prediction can be made by directly studying the I_d of data sets of all measured densities, as

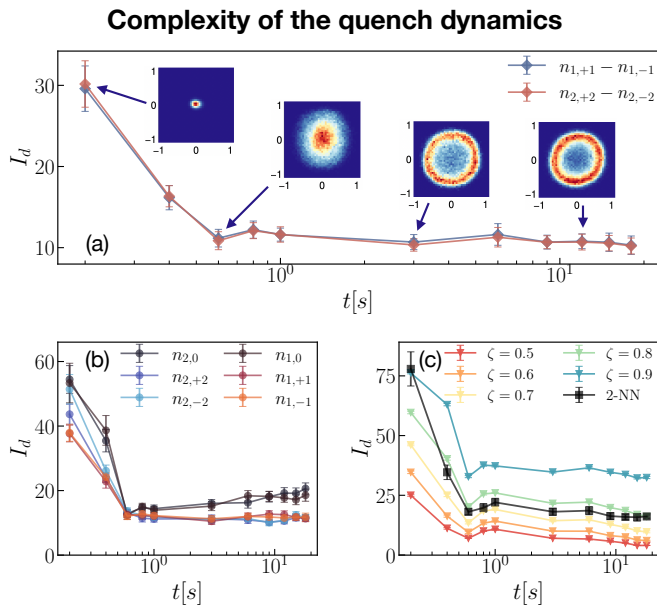


FIG. 3. **Complexity of the dynamics via intrinsic dimension.** Intrinsic dimension as a function of time for (a) the relevant observables, $n_{1,+1} - n_{1,-1}$ and $n_{2,+2} - n_{2,-2}$, (b) all measured densities individually, and (c) joint data sets of all six observables together. In all instances, an initially large I_d quickly decays to smaller values (around $t = 0.6s$), subsequently exhibiting long plateaus. The insets in panel (a) show histograms of the transverse spin in the $F_x - F_y$ plane at selected times. The first drop in the I_d is associated to a grow in the spin length, which remains approximately constant for $t \gtrsim 1s$. In the latter regime a ring-like structure is then observed (illustrated here at $t = 3s, 12s$). Spatial correlations of spin phase excitations exhibit self-similar dynamics in a regime that starts around $t \gtrsim 3s$ [30]. The observed structural simplification of the data strongly correlates with such universal dynamics. Hence, the plateaus in the plot of I_d provide a lower bound for the onset of simpler dynamics and universal scaling. Panel (c) also shows the I_d estimate based on PCA for various values of the cutoff ζ (see main text).

shown in Fig. 3(b), where we observe an overall similar trend. We note, however, that the “irrelevant” observables $n_{1,0}$ and $n_{2,0}$, have a growing I_d , rather than a plateau. This further confirms the relevance predictions based on PCA entropy and information imbalance. Further, in Fig. 3(c) we plot the I_d of joint data sets of the six measured observables together, showing once again the noted trend. In this plot, we also show an I_d estimation based on PCA, which is defined by choosing an *ad hoc* cutoff parameter ζ , for the integrated spectrum of the covariance matrix [38, 51], i.e., $\sum_{k=1}^{I_d} \lambda_k \approx \zeta$. We find that for all considered values of ζ , we recover the same qualitative features as the TWO-NN I_d -estimate. A quantitative agreement can also be achieved for a suitable choice of ζ in the range $0.7 \leq \zeta \leq 0.9$, at the different evolution times. This agreement further confirms the applicability of PCA in our previous analysis and implies

that curvature effects of the data manifold are negligible.

Conclusions.—We have introduced an assumption-free method to diagnose and rank relevant correlations in the dynamics of out-of-equilibrium quantum systems. The method exploits the full spectrum of principal components, as well as recently developed techniques based on information imbalance. We have successfully identified the most relevant operators describing the dynamics of Bose Einstein condensates, confirming previous heuristic approaches (and thus, validating the physical relevance based solely on experimental observations). Utilizing manifold characterization methods, we have also found stable plateaus of the intrinsic dimension of the data sets corresponding to different times, thus providing bounds on the time frame realizing universal quantum dynamics. Our approach is immediately extended to other classes of quantum simulators—including fermion gases and lattice spin models—providing a flexible, assumption-free framework to discover physical phenomena, as well as to validate their functioning. Our work complements recent theoretical approaches with similar goals regarding the identification of relevant observables [54, 55] and characterizing the complexity of quantum dynamics [50, 56, 57].

Acknowledgments. We are grateful to G. Bianconi, B. Lucini, M. Marsili, K. Najafi, S. Pedrielli, and P. Zoller, for discussions and feedback on this and related works. This work was partly supported by the MIUR Programme FARE (MEPH), by QUANTERA DYNAMITE PCI2022-132919, by the PNR MUR project PE0000023-NQSTI, by the Deutsche Forschungsgemeinschaft (DFG, German Research Foundation) through SFB 1225 ISOQUANT – 273811115, and GA677/10-1, as well as under Germany’s Excellence Strategy – EXC-2181/1 – 390900948 (the Heidelberg STRUCTURES Excellence Cluster).

* rverdel@ictp.it

- [1] Immanuel Bloch, Jean Dalibard, and Wilhelm Zwerger, “Many-body physics with ultracold gases,” *Rev. Mod. Phys.* **80**, 885–964 (2008).
- [2] Maciej Lewenstein, Anna Sanpera, and Verónica Ahufinger, *Ultracold Atoms in Optical Lattices: Simulating quantum many-body systems* (Oxford University Press, 2012).
- [3] I. M. Georgescu, S. Ashhab, and Franco Nori, “Quantum simulation,” *Rev. Mod. Phys.* **86**, 153–185 (2014).
- [4] Christian Gross and Immanuel Bloch, “Quantum simulations with ultracold atoms in optical lattices,” *Science* **357**, 995–1001 (2017), <https://www.science.org/doi/pdf/10.1126/science.aal3837>.
- [5] Andrew J. Daley, Immanuel Bloch, Christian Kokail, Stuart Flannigan, Natalie Pearson, Matthias Troyer, and Peter Zoller, “Practical quantum advantage in quantum simulation,” *Nature* **607**, 667–676 (2022).
- [6] Yudong Cao, Jonathan Romero, Jonathan P. Olson,

- Matthias Degroote, Peter D. Johnson, Mária Kieferová, Ian D. Kivlichan, Tim Menke, Borja Peropadre, Nicolas P. D. Sawaya, Sukin Sim, Libor Veis, and Alán Aspuru-Guzik, “Quantum chemistry in the age of quantum computing,” *Chemical Reviews*, **Chemical Reviews** **119**, 10856–10915 (2019).
- [7] Philipp Kunkel, Maximilian Prüfer, Stefan Lannig, Rodrigo Rosa-Medina, Alexis Bonnin, Martin Gärtner, Helmut Strobel, and Markus K. Oberthaler, “Simultaneous readout of noncommuting collective spin observables beyond the standard quantum limit,” *Phys. Rev. Lett.* **123**, 063603 (2019).
- [8] Alexei M. Tsvelik, *Quantum Field Theory in Condensed Matter Physics*, 2nd ed. (Cambridge University Press, 2003).
- [9] Hagen Kleinert, *Collective Classical and Quantum Fields* (WORLD SCIENTIFIC, 2018) <https://www.worldscientific.com/doi/pdf/10.1142/10545>.
- [10] Orly Alter, Patrick O. Brown, and David Botstein, “Singular value decomposition for genome-wide expression data processing and modeling,” *Proceedings of the National Academy of Sciences* **97**, 10101–10106 (2000).
- [11] Roy Varshavsky, Assaf Gottlieb, Michal Linial, and David Horn, “Novel Unsupervised Feature Filtering of Biological Data,” *Bioinformatics* **22**, e507–e513 (2006), <https://academic.oup.com/bioinformatics/article-pdf/22/14/e507/614890/btl214.pdf>.
- [12] Roy Varshavsky, Assaf Gottlieb, David Horn, and Michal Linial, “Unsupervised feature selection under perturbations: meeting the challenges of biological data,” *Bioinformatics* **23**, 3343–3349 (2007), <https://academic.oup.com/bioinformatics/article-pdf/23/24/3343/16861997/btm528.pdf>.
- [13] Aldo Glielmo, Claudio Zeni, Bingqing Cheng, Gábor Csányi, and Alessandro Laio, “Ranking the information content of distance measures,” *PNAS Nexus* **1** (2022).
- [14] Edward Danquah Donkor, Alessandro Laio, and Ali Hassanali, “Do machine-learning atomic descriptors and order parameters tell the same story? the case of liquid water,” *Journal of Chemical Theory and Computation* **0**, null (0), PMID: 36920997, <https://doi.org/10.1021/acs.jctc.2c01205>.
- [15] Elena Facco, Maria d’Errico, Alex Rodriguez, and Alessandro Laio, “Estimating the intrinsic dimension of datasets by a minimal neighborhood information,” *Scientific Reports* **7**, 12140 (2017).
- [16] Elena Facco, Andrea Pagnani, Elena Tea Russo, and Alessandro Laio, “The intrinsic dimension of protein sequence evolution,” *PLOS Computational Biology* **15**, 1–16 (2019).
- [17] Michele Allegra, Elena Facco, Francesco Denti, Alessandro Laio, and Antonietta Mira, “Data segmentation based on the local intrinsic dimension,” *Scientific Reports* **10**, 16449 (2020).
- [18] Aldo Glielmo, Brooke E. Husic, Alex Rodriguez, Cecilia Clementi, Frank Noé, and Alessandro Laio, “Unsupervised learning methods for molecular simulation data,” *Chemical Reviews*, **Chemical Reviews** **121**, 9722–9758 (2021).
- [19] Tanya Strydom, Giulio V. Dalla Riva, and Timothée Poisot, “Svd entropy reveals the high complexity of ecological networks,” *Frontiers in Ecology and Evolution* **9** (2021), 10.3389/fevo.2021.623141.
- [20] Petre Caraiani, “The predictive power of singular value decomposition entropy for stock market dynamics,” *Physica A: Statistical Mechanics and its Applications* **393**, 571–578 (2014).
- [21] Rongbao Gu, Wei Xiong, and Xinjie Li, “Does the singular value decomposition entropy have predictive power for stock market? — evidence from the shenzhen stock market,” *Physica A: Statistical Mechanics and its Applications* **439**, 103–113 (2015).
- [22] Rongbao Gu and Yanmin Shao, “How long the singular value decomposed entropy predicts the stock market? — evidence from the dow jones industrial average index,” *Physica A: Statistical Mechanics and its Applications* **453**, 150–161 (2016).
- [23] Anirban Chakraborti, Hrishidev, Kiran Sharma, and Hirdesh K Pharsai, “Phase separation and scaling in correlation structures of financial markets,” *Journal of Physics: Complexity* **2**, 015002 (2020).
- [24] Jose Alvarez-Ramirez and Eduardo Rodriguez, “A singular value decomposition entropy approach for testing stock market efficiency,” *Physica A: Statistical Mechanics and its Applications* **583**, 126337 (2021).
- [25] G. Espinosa-Paredes, E. Rodriguez, and J. Alvarez-Ramirez, “A singular value decomposition entropy approach to assess the impact of covid-19 on the informational efficiency of the wti crude oil market,” *Chaos, Solitons & Fractals* **160**, 112238 (2022).
- [26] Elizaveta Levina and Peter Bickel, “Maximum likelihood estimation of intrinsic dimension,” in *Advances in Neural Information Processing Systems*, Vol. 17, edited by L. Saul, Y. Weiss, and L. Bottou (MIT Press, 2004).
- [27] S. Gong, V. Boddeti, and A. K. Jain, “On the intrinsic dimensionality of image representations,” in *2019 IEEE/CVF Conference on Computer Vision and Pattern Recognition (CVPR)* (IEEE Computer Society, Los Alamitos, CA, USA, 2019) pp. 3982–3991.
- [28] Phil Pope, Chen Zhu, Ahmed Abdelkader, Micah Goldblum, and Tom Goldstein, “The intrinsic dimension of images and its impact on learning,” in *International Conference on Learning Representations* (2021).
- [29] Xiaojing Weng, Altai Perry, Michael Maroun, and Luat T. Vuong, “Singular value decomposition and entropy dimension of fractals,” in *2022 International Conference on Image Processing, Computer Vision and Machine Learning (ICICML)* (2022) pp. 427–431.
- [30] Maximilian Prüfer, Torsten V. Zache, Philipp Kunkel, Stefan Lannig, Alexis Bonnin, Helmut Strobel, Jürgen Berges, and Markus K. Oberthaler, “Experimental extraction of the quantum effective action for a non-equilibrium many-body system,” *Nature Physics* **16**, 1012–1016 (2020).
- [31] Maximilian Prüfer, Philipp Kunkel, Helmut Strobel, Stefan Lannig, Daniel Linnemann, Christian-Marcel Schmied, Jürgen Berges, Thomas Gasenzer, and Markus K. Oberthaler, “Observation of universal dynamics in a spinor bose gas far from equilibrium,” *Nature* **563**, 217–220 (2018).
- [32] Yuki Kawaguchi and Masahito Ueda, “Spinor bose–einstein condensates,” *Physics Reports* **520**, 253–381 (2012), spinor Bose–Einstein condensates.
- [33] J. Berges, K. Boguslavski, S. Schlichting, and R. Venugopalan, “Universality far from equilibrium: From superfluid bose gases to heavy-ion collisions,” *Phys. Rev. Lett.* **114**, 061601 (2015).
- [34] Sebastian Erne, Robert Bücken, Thomas Gasenzer,

- Jürgen Berges, and Jörg Schmiedmayer, “Universal dynamics in an isolated one-dimensional bose gas far from equilibrium,” *Nature* **563**, 225–229 (2018).
- [35] Jake A. P. Glidden, Christoph Eigen, Lena H. Dogra, Timon A. Hilker, Robert P. Smith, and Zoran Hadzibabic, “Bidirectional dynamic scaling in an isolated bose gas far from equilibrium,” *Nature Physics* **17**, 457–461 (2021).
- [36] L. E. Sadler, J. M. Higbie, S. R. Leslie, M. Vengalattore, and D. M. Stamper-Kurn, “Spontaneous symmetry breaking in a quenched ferromagnetic spinor bose-einstein condensate,” *Nature* **443**, 312–315 (2006).
- [37] Supplemental material for details on the information imbalance method, the relevance ranking of further combinations of observables, the linear fit used to estimate the intrinsic dimension with the TWO-NN method, and the subsampling technique used to estimate error bars.
- [38] Ian Jolliffe, “Principal component analysis,” in *Encyclopedia of Statistics in Behavioral Science* (John Wiley & Sons, Ltd, 2005).
- [39] Pankaj Mehta, Marin Bukov, Ching-Hao Wang, Alexandre G.R. Day, Clint Richardson, Charles K. Fisher, and David J. Schwab, “A high-bias, low-variance introduction to machine learning for physicists,” *Physics Reports* **810**, 1–124 (2019), a high-bias, low-variance introduction to Machine Learning for physicists.
- [40] The normalized eigenvalue $\tilde{\lambda}_n$ is interpreted as the *proportion of total variance* that is accounted for by the n -th principal component.
- [41] C. E. Shannon, “A mathematical theory of communication,” *The Bell System Technical Journal* **27**, 379–423 (1948).
- [42] Here we only consider the simplest combinations of the relevant observables $n_{1,+1}$ and $n_{1,-1}$. However, we note that, in principle, we cannot disregard that other, more complicated, combinations may yield even lower values of S_{PCA} .
- [43] Dimitris N. Politis, Joseph P. Romano, and Michael Wolf, *Subsampling*, 1st ed. (Springer New York, 1999).
- [44] Jun Shao and Dongsheng Tu, *The Jackknife and Bootstrap*, 1st ed. (Springer New York, 1995).
- [45] P. Campadelli, E. Casiraghi, C. Ceruti, and A. Rozza, “Intrinsic dimension estimation: Relevant techniques and a benchmark framework,” *Mathematical Problems in Engineering* **2015**, 759567 (2015).
- [46] Francesco Camastra and Antonino Staiano, “Intrinsic dimension estimation: Advances and open problems,” *Information Sciences* **328**, 26–41 (2016).
- [47] Ming Li and Paul Vitányi, *An Introduction to Kolmogorov Complexity and Its Applications*, 3rd ed. (Springer New York, 2009).
- [48] L. Staiger, “Kolmogorov complexity and hausdorff dimension,” *Information and Computation* **103**, 159–194 (1993).
- [49] Vittorio Vitale, Tiago Mendes-Santos, Alex Rodriguez, and Marcello Dalmonte, “Topological kolmogorov complexity and the berezinskii-kosterlitz-thouless mechanism,” (2023), [arXiv:2305.05396 \[cond-mat.stat-mech\]](https://arxiv.org/abs/2305.05396).
- [50] T. Mendes-Santos, M. Schmitt, A. Angelone, A. Rodriguez, P. Scholl, H. J. Williams, D. Barredo, T. Lahaye, A. Browaeys, M. Heyl, and M. Dalmonte, “Wave function network description and Kolmogorov complexity of quantum many-body systems,” [arXiv e-prints](https://arxiv.org/abs/2301.13216), [arXiv:2301.13216](https://arxiv.org/abs/2301.13216) (2023), [arXiv:2301.13216 \[cond-mat.quant-gas\]](https://arxiv.org/abs/2301.13216).
- [51] T. Mendes-Santos, X. Turkeshi, M. Dalmonte, and Alex Rodriguez, “Unsupervised learning universal critical behavior via the intrinsic dimension,” *Phys. Rev. X* **11**, 011040 (2021).
- [52] T. Mendes-Santos, A. Angelone, Alex Rodriguez, R. Fazio, and M. Dalmonte, “Intrinsic dimension of path integrals: Data-mining quantum criticality and emergent simplicity,” *PRX Quantum* **2**, 030332 (2021).
- [53] Xhek Turkeshi, “Measurement-induced criticality as a data-structure transition,” *Phys. Rev. B* **106**, 144313 (2022).
- [54] Cole Miles, Annabelle Bohrdt, Ruihan Wu, Christie Chiu, Muqing Xu, Geoffrey Ji, Markus Greiner, Kilian Q. Weinberger, Eugene Demler, and Eun-Ah Kim, “Correlator convolutional neural networks as an interpretable architecture for image-like quantum matter data,” *Nature Communications* **12**, 3905 (2021).
- [55] A. Bohrdt, S. Kim, A. Lukin, M. Rispoli, R. Schittko, M. Knap, M. Greiner, and J. Léonard, “Analyzing nonequilibrium quantum states through snapshots with artificial neural networks,” *Phys. Rev. Lett.* **127**, 150504 (2021).
- [56] Markus Schmitt and Zala Lenarčič, “From observations to complexity of quantum states via unsupervised learning,” *Phys. Rev. B* **106**, L041110 (2022).
- [57] Heitor P. Casagrande, Bo Xing, Marcello Dalmonte, Alex Rodriguez, Vinitha Balachandran, and Dario Poletti, “Complexity of spin configurations dynamics due to unitary evolution and periodic projective measurements,” [arXiv e-prints](https://arxiv.org/abs/2305.03334), [arXiv:2305.03334](https://arxiv.org/abs/2305.03334) (2023), [arXiv:2305.03334 \[cond-mat.stat-mech\]](https://arxiv.org/abs/2305.03334).

Supplemental Material

MORE ON INFORMATION IMBALANCE

In the following we summarize the main ideas that lead to Eq. (3) in the main text, but the reader is referred to Ref. [13] for a more detailed explanation. The notion of *information imbalance* refers to a statistical test aimed at assessing the relative information content of different distance measures defined on the same data space [13, 14]. This is done by analyzing the *ranks* of first nearest neighbors of each point. More specifically, given a finite data set $\mathbf{M} = \{\vec{\mathcal{N}}_i\}_{i=1}^{N_r}$ and two distance measures $D_A(\vec{\mathcal{N}}_i, \vec{\mathcal{N}}_j)$ and $D_B(\vec{\mathcal{N}}_i, \vec{\mathcal{N}}_j)$, we can rank the neighbors of a point $\vec{\mathcal{N}}_i$, in the two spaces under consideration, by sorting, from smallest to largest, the pairwise distances between such a point and the rest of points using the corresponding metric. These rankings are encoded in the so-called rank matrices $R_{i,j}^{A/B}$. Thus, for example, $R_{i,j}^A = 1$ if $\vec{\mathcal{N}}_j$ is the 1st nearest neighbor of $\vec{\mathcal{N}}_i$ in space A , $R_{i,j}^A = 2$ if $\vec{\mathcal{N}}_j$ is the 2nd nearest neighbor of $\vec{\mathcal{N}}_i$, etc. The key insight of this method is the fact that the full correlation structure between the two metrics under study is essentially captured by the conditional rank distribution $p(R^B|R^A = 1)$, that is, the probability distribution of the ranks $R_{i,j}^B$ in space B restricted to those pairs (i, j) for which $R_{i,j}^A = 1$ (i.e., the pairs of nearest neighbors in A). Then, the closer this distribution is to a delta function peaked at 1, the more information (at the level of local neighborhoods) about space B is contained within space A . The deviation of $p(R^B|R^A = 1)$ from such a delta function is quantified by the conditional expectation $\langle R^B|R^A = 1 \rangle$, which is used to define the information imbalance from space A to space B , namely

$$\Delta(A \rightarrow B) = \frac{2}{N_r} \langle R^B|R^A = 1 \rangle = \frac{2}{N_r^2} \sum_{i,j:R_{i,j}^A=1} R_{i,j}^B. \quad (\text{S1})$$

In the limit case where the two spaces are completely equivalent (meaning that first nearest neighbors in A are exactly the same as those in B), we have that $\sum_{j:R_{i,j}^A=1} R_{i,j}^B = 1$ (for a given i), and hence $\sum_{i,j:R_{i,j}^A=1} R_{i,j}^B = N_r$. Therefore, the information imbalance in Eq. (S1), $\Delta(A \rightarrow B)$ vanishes as $1/N_r$. A vanishing information imbalance indicates that A can fully predict B in the sense specified above. In the extremely opposite case in which the two spaces are completely independent, we have that $\sum_{j:R_{i,j}^A=1} R_{i,j}^B = \frac{1}{N_r-1} \cdot \frac{1}{2} N_r(N_r - 1) = \frac{N_r}{2}$ and hence $\sum_{i,j:R_{i,j}^A=1} R_{i,j}^B = \frac{N_r^2}{2}$. Therefore, the resulting information imbalance is $\Delta(A \rightarrow B) = 1$, implying that A cannot predict B . Finally, we note that, due to its own definition, the information imbalance is asymmetric; therefore, one can study predictability between the two considered distances in both directions.

RELEVANCE RANKING VIA S_{PCA} AND INFORMATION IMBALANCE: FURTHER COMBINATIONS

In this section, we show the ranking of further combinations of operators. As explained in the main text, we analyse joint data sets formed by concatenating horizontally measured data sets. Thus, for example, $n_{1,+1} \parallel n_{1,-1}$ refers to a data set for which we have concatenated horizontally the data sets corresponding to the observables $n_{1,+1}$ and $n_{1,-1}$. Complementing Fig. 2 of the main text, in Figs. S1 and S2, we show the ranking of all joint data sets formed by two observables, according to S_{PCA} and $\Delta(A \rightarrow B)$, respectively. As mentioned in the main text, the joint data sets with a lower value of S_{PCA} , throughout almost the whole evolution, are $n_{1,+1} \parallel n_{1,-1}$ and $n_{2,+2} \parallel n_{2,-2}$ (\star markers in Fig. S1). These pairs of observables are indeed the most relevant ones to describe the physics of the quenched system. We also note that the joint data set $n_{1,0} \parallel n_{2,0}$ is the one with the largest PCA entropy, and hence is the “least” informative one. This is also in agreement with physical considerations as the populations in the respective substates are only important to normalize properly the collective transverse spin variable (see Eq. (1) in the main text). Information imbalance—which does not rely on a linear transformation as does PCA, but on ranks of nearest neighbors—provides a complementary view on the relevance of the analysed observations. Let us recall that $\Delta(A \rightarrow B) \sim 0$ means that A can reliably predict B , whereas $\Delta(A \rightarrow B) \sim 1$ implies that A cannot predict B . Here, we measure the information imbalance from a space A of features corresponding to joint data sets of two observables, to the space B of features corresponding to the joint data set of all six observables together. In Fig. S2, we observe that the joint data set with the largest information imbalance (smallest information content) is $n_{1,0} \parallel n_{2,0}$, in full agreement with the ranks obtained using the PCA entropy. Next, we observe that the joint data sets with the smallest information imbalance are not $n_{1,+1} \parallel n_{1,-1}$ and $n_{2,+2} \parallel n_{2,-2}$, but those where features from these two relevant pairs are combined, namely: $n_{1,+1} \parallel n_{2,+2}$, $n_{1,+1} \parallel n_{2,-2}$, $n_{1,-1} \parallel n_{2,+2}$, and $n_{1,-1} \parallel n_{2,-2}$ (markers with darker color in Fig. S2). In fact, any of these

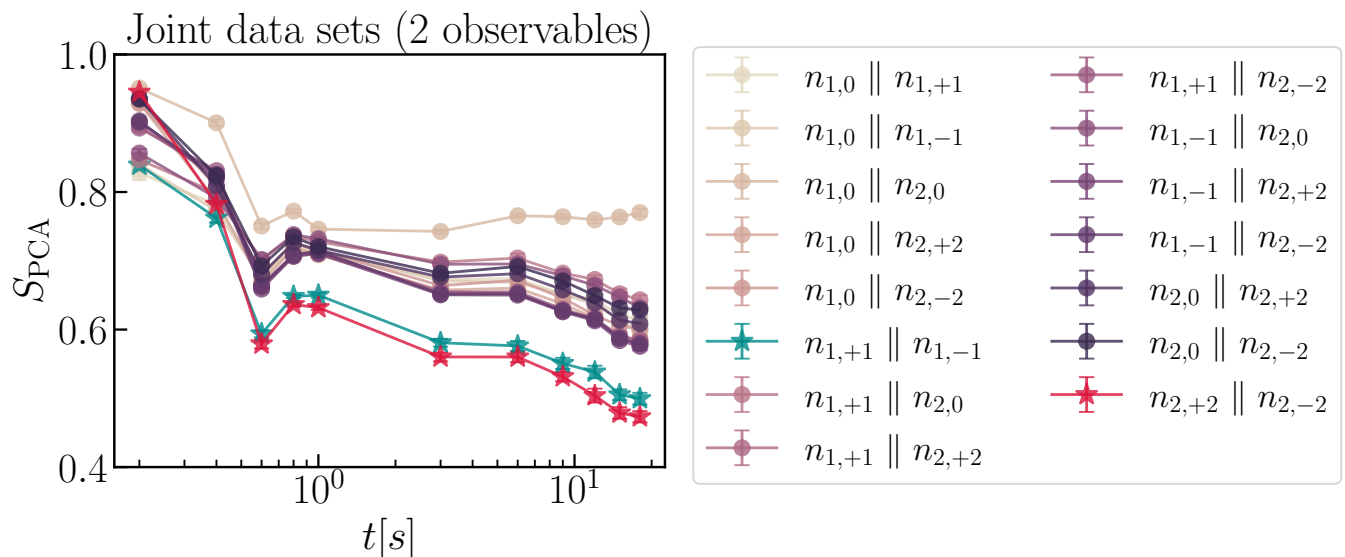


FIG. S1. PCA entropy of joint data sets of two observables. This plot shows the results for all joint data sets of two observables (cf. Fig. 2(a.2) of the main text).

four joint data sets can predict almost entirely the full space of features, since $\Delta(A \rightarrow B) \sim 0$ for such data sets. The meaning of this observation is that in order to predict better the full space of features (given by the coordinates of the joint data set of the measured six observables), one needs to consider features from both of the identified relevant pairs $n_{1,+1} \parallel n_{1,-1}$ and $n_{2,+2} \parallel n_{2,-2}$.

Similar conclusions apply if one considers groups of more than two observables. This is illustrated here for groups of four observables (quadruplets) in Figs. S3 and S4. In terms of PCA entropy the most relevant joint data set is the one that combines the features of the two relevant pairs, namely, $n_{1,+1} \parallel n_{1,-1} \parallel n_{2,+2} \parallel n_{2,-2}$ (\star markers in Fig. S3). We note however that in this case the relative difference in PCA entropy is not as pronounced as in the case of single or two observables. Regarding information imbalance, we observe once again those joint data sets that combine features from the two relevant pairs can predict almost entirely the full space of features. There are indeed only two combinations that only involve features from a single relevant pair (plus the two “irrelevant” observables $n_{1,0}$ and $n_{2,0}$), namely, $n_{1,0} \parallel n_{1,+1} \parallel n_{1,-1} \parallel n_{2,0}$ and $n_{1,0} \parallel n_{2,0} \parallel n_{2,+2} \parallel n_{2,-2}$ (square markers in Fig. S4), which clearly have a significantly larger information imbalance compared to the rest.

LINEAR FIT TO ESTIMATE I_d FROM THE EMPIRICAL CUMULATES IN THE TWO-NN METHOD

In this section, we show examples of the linear fitting procedure used to estimate the value of the intrinsic dimension in the TWO-NN method; see Eq. (4) in the main text. In Fig. S5, we show the empirical cumulative distributions of the ratios $\mu_i = r_{i_2}/r_{i_1}$, sorted in ascending order, for the observable $n_{2,+2} - n_{2,-2}$, at all evolution times. If the condition of constant density in the range of first two nearest neighbors holds, a plot of the resulting points $\{\ln(\mu), -\ln[1 - F_{\text{emp}}(\mu)]\}$ will be a line that passes through the origin and whose slope gives the estimated value of I_d . Verifying that the empirical cumulates are indeed consistent with a Pareto distribution as described above, is the first step to guarantee the applicability of the TWO-NN method. Besides, on its own, this kind of plot is also very informative about the local structure of complicated data manifolds.

SUBSAMPLING ERROR ESTIMATION

Due to the limited number of realizations used in the present analysis, we opted for using a technique known as subsampling [43, 44] to have a sensible estimation of the statistical errors. The subsampling algorithm is described below.

At a given time and for a given measured observable, we have $N_r = 225$ independent realizations forming our data

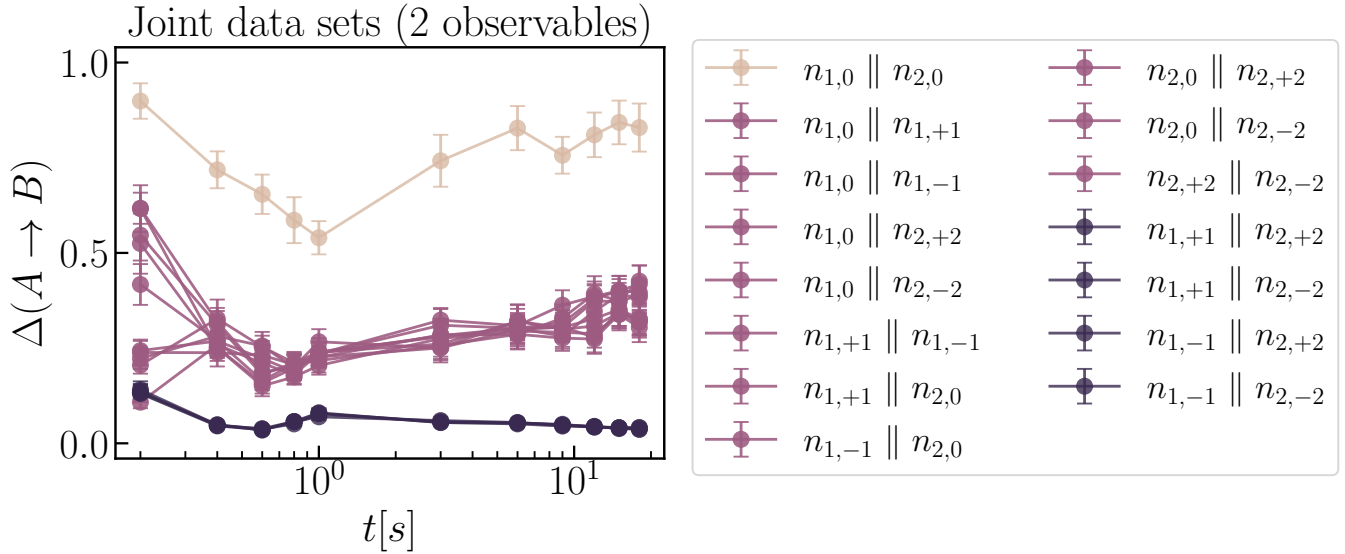


FIG. S2. Information imbalance of joint data sets of two observables. This plot shows the results for all joint data sets of two observables (cf. Fig. 2(a.5) of the main text). Note that the points corresponding to the joint data sets $n_{1,+1} \parallel n_{2,+2}$, $n_{1,+1} \parallel n_{2,-2}$, $n_{1,-1} \parallel n_{2,+2}$, and $n_{1,-1} \parallel n_{2,-2}$, lie basically on top of each other (they are equally informative), with an information imbalance $\Delta(A \rightarrow B) \sim 0$. These four data sets combine features of the two relevant pairs $\{n_{1,+1}, n_{1,-1}\}$ and $\{n_{2,+2}, n_{2,-2}\}$.

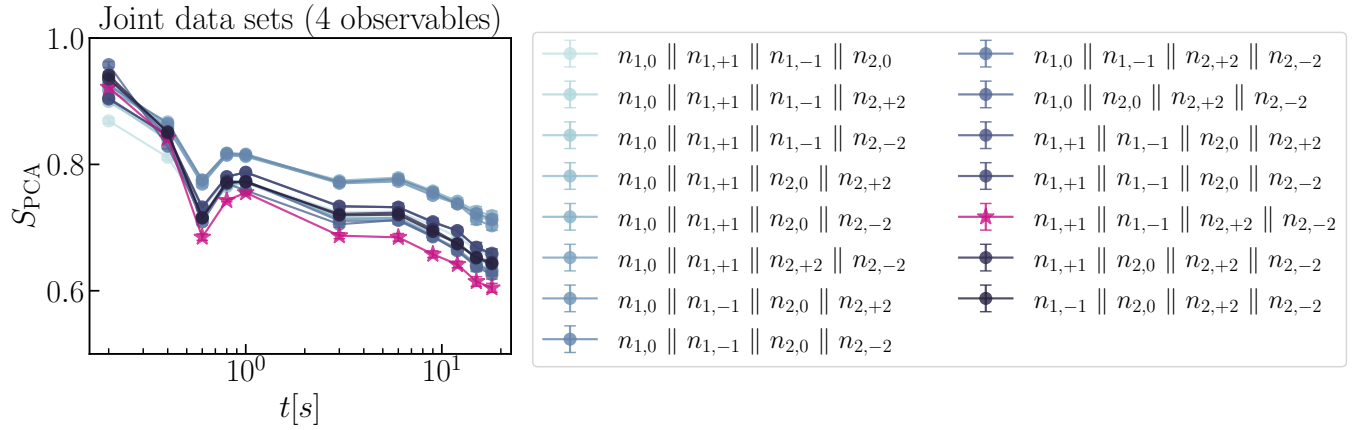


FIG. S3. PCA entropy of joint data sets of four observables. The joint data set with the smallest PCA entropy is the one that combines the two relevant pairs (\star markers).

set, that is, $\mathbf{M} = \{\tilde{\mathcal{N}}_i\}_{i=1}^{N_r}$, where for simplicity we have omitted the indices labeling the observable and the evolution time. Using these data we compute a certain numerical statistic ϑ . Given two preset integers b and $q < N_r$, the subsampling analysis proceeds as follows:

1. Form b random ‘batches’ (subsamples) of data by drawing $q < N_r$ points at random but *without* replacement from the data set $\{\tilde{\mathcal{N}}_1, \tilde{\mathcal{N}}_2, \dots, \tilde{\mathcal{N}}_{N_r}\}$.

2. Estimate the statistic of interest on each subsample, that is, ϑ_i , for $i \in \{1, \dots, b\}$.

3. Compute the subsample mean $\bar{\vartheta} = \frac{1}{b} \sum_{i=1}^b \vartheta_i$. The standard error can then be estimated as follows

$$\text{SE} \approx \sqrt{\frac{q}{N_r - q}} \cdot \sqrt{\frac{1}{b} \sum_{i=1}^b (\vartheta_i - \bar{\vartheta})^2}, \quad (\text{S2})$$

This formula is known as the delete- d Jackknife standard error estimator (with stochastic subsampling) [43, 44].

While formally this method requires $q/N_r \rightarrow 0$, $q \rightarrow \infty$, and $b \rightarrow \infty$ as $N_r \rightarrow \infty$ (so that the distribution of the

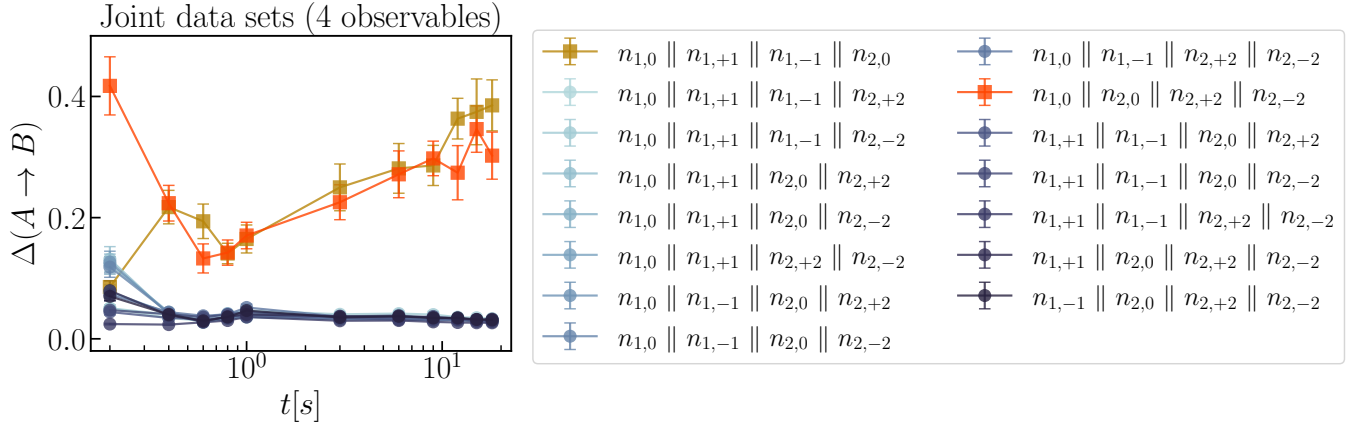


FIG. S4. Information imbalance of joint data sets of four observables. All joint data sets that combine features from the two relevant pairs $\{n_{1,+1}, n_{1,-1}\}$ and $\{n_{2,+2}, n_{2,-2}\}$ have a very small information imbalance. Instead, the joint data sets that only use features from one of the relevant pairs cannot predict so well the the full space of features. The latter are indicated with square markers in this plot.

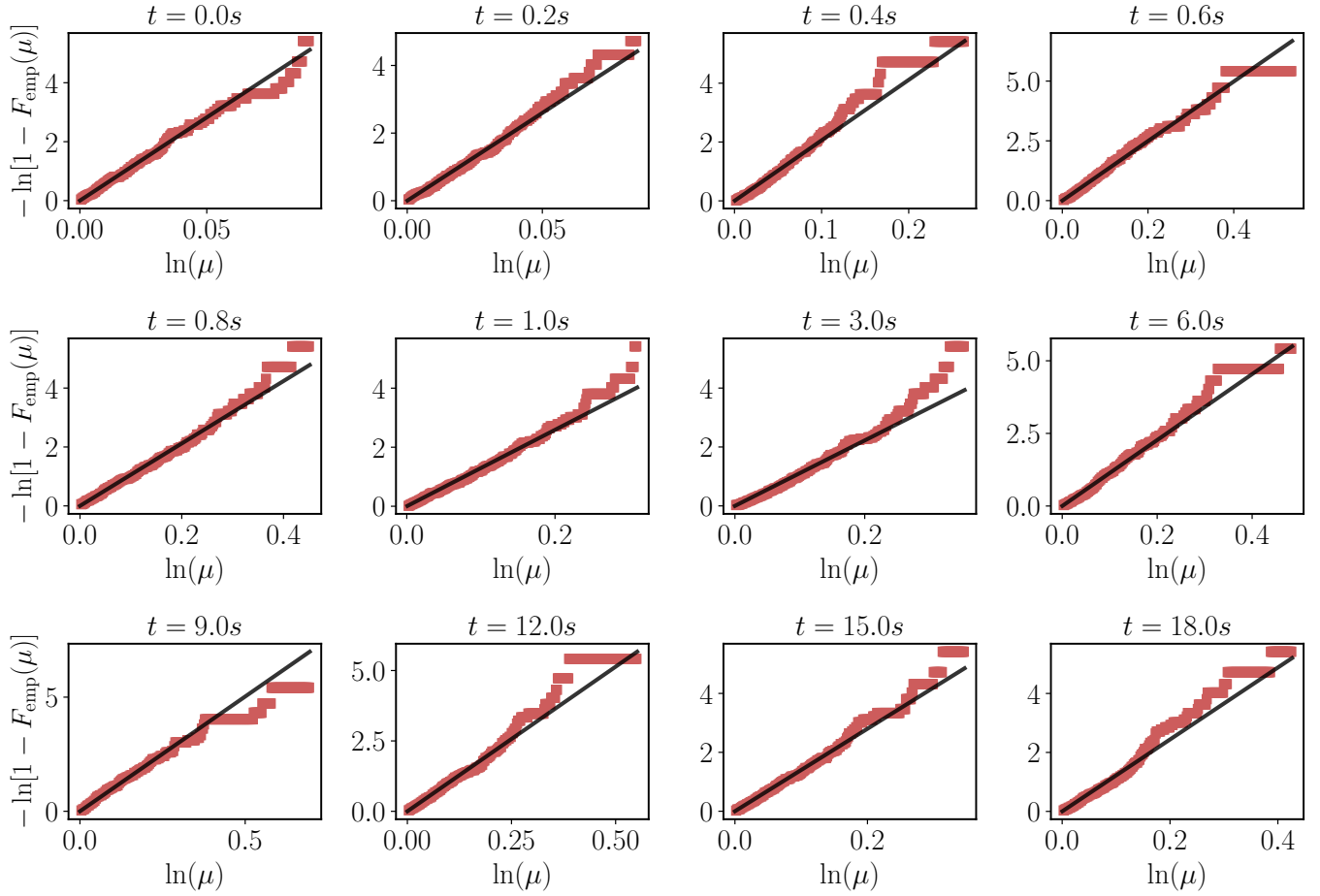


FIG. S5. Empirical cumulative distributions at all evolution times for the data sets corresponding to the relevant observable $n_{2,+2} - n_{2,-2}$. The black curve show the linear fit according to Eq. (4) in the main text, whose slope gives the estimated value of I_d . This procedure is valid as long as the empirical cumulative distribution function is consist with a Pareto distribution, at least over a significant range of values of $\ln(\mu)$, as is the case here.

ϑ_i converges to the sampling distribution of ϑ), in practice the choice of these parameters is problem specific. In

our analysis, we did not find significant changes for $b \geq 30$. Hence, we fixed $b = 30$. Furthermore, to compute a meaningful statistic on each subsample, we set $q = 100$.

We used this method as sampling is performed *without* replacement. This is important as the TWO-NN algorithm used to estimate the I_d works under the assumption of no repetitions among the data points.